Topochemical fluorination of n = 2 Ruddlesden–Popper type $Sr_3Ti_2O_7$ to $Sr_3Ti_2O_5F_4$ and its reductive defluorination

Wissel, Kerstin; Vogel, Tobias; Dasgupta, Subratik; Fortes, Andrew Dominic; Slater, Peter; Clemens, Oliver

DOI:
10.1021/acs.inorgchem.9b02783

Document Version
Peer reviewed version

Citation for published version (Harvard):
Wissel, K, Vogel, T, Dasgupta, S, Fortes, AD, Slater, P & Clemens, O 2020, 'Topochemical fluorination of *n* = 2 Ruddlesden–Popper type $Sr_3Ti_2O_7$ to $Sr_3Ti_2O_5F_4$ and its reductive defluorination', *Inorganic Chemistry*, vol. 59, no. 2, pp. 1153-1163. https://doi.org/10.1021/acs.inorgchem.9b02783

Topochemical Fluorination of n = 2 Ruddlesden-Popper type $Sr_3Ti_2O_7$ to $Sr_3Ti_2O_5F_4$ and its reductive Defluorination

Kerstin Wissel[a], Tobias Vogel[b], Supratik Dasgupta[b], Andrew Dominic Fortes[c], Peter. R. Slater[d], Oliver Clemens[a,e]*

[a] Technische Universität Darmstadt, Institut für Materialwissenschaft, Fachgebiet Materialdesign durch Synthese, Alarich-Weiss-Straße 2, 64287 Darmstadt, Germany

[b] Technische Universität Darmstadt, Institut für Materialwissenschaft, Fachgebiet Dünne Schichten, Alarich-Weiss-Straße 2, 64287 Darmstadt, Germany

[c] ISIS Facility, Rutherford Appleton Laboratory, Harwell Science and Innovation Campus, Didcot, Oxfordshire OX11 0QX, United Kingdom

[d] School of Chemistry, University of Birmingham, Birmingham B15 2TT, United Kingdom

[e] Karlsruhe Institute of Technology, Institut für Nanotechnologie, Hermann-von-Helmholtz-Platz 1, 76344 Eggenstein-Leopoldshafen, Germany

* Corresponding Author
Fax: +49 6151 16 20965
E-Mail: oliver.clemens@md.tu-darmstadt.de

Abstract

Within this study, we show that a sequence of substitutive topochemical fluorination of the n = 2 Ruddlesden-Popper type compounds $Sr_3Ti_2O_7$ to $Sr_3Ti_2O_5F_4$ followed by reductive topochemical defluorination reactions between the oxyfluoride and the reducing agent sodium hydride allows for a substantial reduction of the oxidation state of Ti due to selective extraction and hydride substitution of fluoride ions. The oxyfluoride $Sr_3Ti_2O_5F_4$ has been synthesized and characterized structurally for the first time. The defluorination experiments have been conducted at temperatures as low as 300 °C enabling also the reduction of this metastable compound. The evolution of phase fractions and unit cell volumes of various reduced phases as well as of side products have been monitored by an X-ray diffraction study as a function of the amount of sodium hydride used. Strong structural changes within the reduced phases, involving considerable decreases in the *c* lattice parameters partly accompanied by symmetry lowering, have been observed. To gain a deeper understanding of the structural changes, selected reduction reaction products have been further investigated by coupled analysis of X-ray and neutron powder diffraction data. Moreover, changes in the oxidation state of Ti have been studied using magnetic measurements and X-ray photoelectron spectroscopy examining differences between the bulk and the surface properties. Additionally, similarities and differences between previously published results on the topochemical defluorination of the n = 1 Ruddlesden-Popper type compound $Sr_2TiO_3F_2$ are discussed.

Keywords

Topochemical fluorination, topochemical defluorination, Ruddlesden-Popper structure, low-valent titanium

1. Introduction

Topochemical methods for the fluorination of oxide materials have been intensively studied due to the strong impact of fluoride incorporation on the crystal structure and electronic properties of materials. Concerning this, low-temperature fluorination routes are of particular interest since they allow for the synthesis of new metastable compounds, which cannot be obtained using more conventional high-temperature synthesis methods. [1-4] A large variety of fluorinating agents have been used for topochemical reactions including F_2, NF_3, NH_4F, MF_2 (M=Cu, Zn, Ni, Ag), XeF_2 as well as fluorinated polymers (PTFE, PVDF). [2, 3] Additionally fluorination can be achieved using electrochemical methods. [5] In contrast, the “reverse” principle of topochemical defluorination to selectively extract fluorine out of oxyfluorides has not been investigated extensively so far. Recently, we introduced a reductive defluorination method that allows for the extraction of fluoride out of an oxyfluoride matrix by chemical means via a low-temperature route. [6]

Ruddlesden-Popper (RP) type strontium titanates $Sr_{n+1}Ti_nO_{3n+1}\square_2$ (n = 1, 2, 3, ∞) have gained much attention due to their ferroelectric and dielectric properties. [7, 8] Additionally, they show a vivid reactivity for a broad range of topochemical modifications of the anion sublattice, which we have already examined on the n = 1 member of the strontium titanate homologous series [6]: The RP type precursor oxide Sr_2TiO_4 has been modified in a two-step process, in which Sr_2TiO_4 is first substitutive fluorinated to $Sr_2TiO_3F_2$. In a subsequent step, $Sr_2TiO_3F_2$ is reductively defluorinated to $Sr_2TiO_3F_{2-x}H_y$. The reduction is based on the reaction between the oxyfluoride and sodium hydride (NaH) at temperatures as low as 300 °C. The oxyfluoride is reduced, leading to the formation of NaF. It was shown that using this route, $Sr_2TiO_3F_2$ can be successfully reduced to compounds containing low-valent Ti.

Conceptionally, a general reaction scheme related to the structural conditions within RP type strontium titanates can be imagined. $Sr_{n+1}Ti_nO_{3n+1}\square_2$ is composed of n $SrTiO_3$ perovskite layers interleaved with one SrO rock salt layer. Hence, the higher the dimensionality n, the more perovskite layers are present and the structures can be considered as being more closely related to the perovskite structure. This, in turn, means that the relative amount of SrO rock salt layers and, therefore, interstitial vacancies □ decrease. These interstitial sites play an important role for the substitutive topochemical fluorination of RP oxides to the respective oxyfluorides, since they can accommodate additional anions (up to two anions X per unit cell according to $Sr_{n+1}Ti_nO_{2n}^{equ}O_{n+1}^{ap}X_2^{int}$ (equ = equatorial, ap =apical, int = interlayer)). For substitutive fluorination reactions (substitution of one oxide ion by two fluoride ions, i.e. under maintenance of the Ti^{4+} oxidation state), this implies that fluorinated phases such as $Sr_{n+1}Ti_nO_{3n+1-x}F_{2x}$ ($0 < x \leq 2$) could be formed in theory. Then, the degree of introduced fluoride ions per Ti cation also affects the lowest oxidation state of Ti, which can be obtained after the subsequent reduction: Overall, the ratio between the two interstitial fluoride ions, which can be extracted, and the number of n Ti cations decreases with increasing n. This leads to smaller possible degrees of reduction for higher order members of the homologous series, which might in turn have an impact on the stability of the formed phases.

Within this study, we report on the formation of $Sr_3Ti_2O_5F_4$ via a topochemical fluorination of n = 2 RP type $Sr_3Ti_2O_7$ using polyvinylidene difluoride (PVDF). Structural analysis confirms that the formation of $Sr_3Ti_2O_5F_4$ can be explained as a substitution and insertion process, in which two oxide ions are replaced by four fluoride ions. Further, topochemical reactions with NaH lead to a significant extraction of fluoride as well as fluoride-hydride exchange, which are accompanied by considerable changes of the crystal structures and magnetic properties, highlighting the possibility to apply combined topochemical reaction schemes for property engineering of higher order RP type compounds.

2. Experimental

2.1 Synthesis of $Sr_3Ti_2O_7$ and $Sr_3Ti_2O_5F_4$

The precursor oxide $Sr_3Ti_2O_7$ was synthesized by a solid-state reaction between high purity $SrCO_3$ (≥ 98 %, Sigma-Aldrich, Germany) and TiO_2 (nanopowder, ≥ 99.7 %, anatase, Sigma-Aldrich, Germany). Stoichiometric amounts of the starting materials were mixed using a ball mill (250 RPM, 30 min) and heated to 1250 °C for 24 h in air. After regrinding, the heat treatment was repeated.

For the chemical fluorination of $Sr_3Ti_2O_7$ to $Sr_3Ti_2O_5F_4$, the oxide was mixed with the fluorination agent polyvinylidene fluoride (PVDF, Sigma-Aldrich, Germany) with 5 % excess using mortar and pestle and heated to 370 °C for 24 h under air.

2.2 Topochemical Reduction Reactions of $Sr_3Ti_2O_5F_4$

The reduction of $Sr_3Ti_2O_5F_4$ was achieved using NaH (dry, 95 %, Sigma-Aldrich, Germany) as reducing agent. The oxyfluoride was intimately ground with NaH using mortar and pestle in an Ar-filled glovebox. The molar ratios of the oxyfluoride and NaH were chosen according to $Sr_3Ti_2O_5F_4$ + x NaH of with ($0.5 \leq x \leq 4$). The obtained mixtures were subsequently filled into corundum crucibles, sealed in stainless steel reactors and heated to 300 °C for 48 h. The synthesis temperature of 300 °C used for the reductions was chosen deliberately and is based on our experience gained in the reduction of the n =1 member $Sr_2TiO_3F_2$ [6]. It was found that too low temperatures (< 280 °C) result in large amounts of unreacted NaH and unreacted $Sr_2TiO_3F_2$ due to the kinetic inhibition of the reaction. Higher temperatures, on the other hand, lead to the increased decomposition of the metastable [9] oxyfluoride compound. Therefore, the chosen reaction temperature and time can be regarded as an optimized experimental setting for the defluorination reaction. After the reduction reaction, the reactor was opened inside an Ar-filled glovebox to remove the sample.

2.3 Re-oxidation of Reduction Products

Reacted mixtures $Sr_3Ti_2O_5F_4$ + x NaH with x = 2 and x = 4 were intentionally re-oxidized by heating them to 350 °C for 4 h in air.

2.4 Diffraction Experiments

X-ray diffraction (XRD) patterns were recorded on a Bruker D8 Advance in Bragg-Brentano geometry with Cu K_α radiation and a VANTEC detector. For the high quality X-ray patterns of $Sr_3Ti_2O_7$, $Sr_3Ti_2O_5F_4$ and the

reduction products $Sr_3Ti_2O_5F_4$ + x NaH (0.5 ≤ x ≤ 4), the samples were measured in a 2θ-range between 20° and 130° using a variable divergence slit of 4 mm for ~ 15 h. The reduction products were measured inside low background airtight specimen holders (Bruker A100B36/B37) which were sealed inside an Ar-filled glovebox.

Time of flight (TOF) powder neutron diffraction (NPD) data were recorded on the HRPD high resolution diffractometer at the ISIS pulsed spallation source (Rutherford Appleton Laboratory, UK). [10-11] ~ 1.5 g of powder samples were loaded into 6 mm diameter thin-walled, airtight sealed cylindrical vanadium sample cans and data were collected at ambient temperature for 40 μAh ($Sr_3Ti_2O_5F_4$), 180 μAh ($Sr_3Ti_2O_5F_4$ + 4NaH) and 240 μAh ($Sr_3Ti_2O_5F_4$ + 2NaH) proton beam current to the ISIS target (corresponding to ~ 1, ~ 4.5 and ~ 6 hours of beam time, respectively). The TOF data were normalized to the incident spectrum and corrected for detector efficiency by reference to a V:Nb standard using the Mantid suite of diffraction utilities. [12]

Analysis of diffraction data was performed using the Rietveld method with the program TOPAS V. 5.0 [13, 14] using the whole 2θ-range as well as the data recorded on all diffraction banks of the TOF diffractometer. The instrumental intensity distribution of the XRD and NPD instruments were determined empirically from a sort of fundamental parameters set [15] using a reference scan of LaB_6 (NIST 660a) and silicon (NIST SRM 640c), respectively. The microstructural parameters (crystallite size and strain broadening) were refined to adjust the peak shapes. Thermal displacement parameters were constrained to be the same for all atoms of all phases to minimize quantification errors and correlation with occupancy parameters.

2.5 Scanning Electron Microscopy

The scanning electron microscopy (SEM) images were recorded using the secondary electron detector of a Philips XL30 FEG scanning electron microscope operating at 10 keV. Prior to the measurements, the samples was sputtered with ~ 10 nm of Au.

2.6 Elemental Analysis

Elemental analysis was performed on a VarioEL III CHN (Elementar). The samples were burned in Sn boats under oxygen and the evolving gases were gas chromatographically separated and analyzed quantitatively with a thermal conductivity detector. The hydride content was determined as the mean of four measurements.

2.7 Magnetic Measurements

Magnetic characterization was performed with a Quantum Design MPMS. Powder samples were contained in gelatin capsules and mounted in a straw. Field-cooled (FC) and zero-field-cooled (ZFC) curves were measured from 5 K to 250 K with an applied field of $\mu_0 H$ = 1T. The magnetization measurements were corrected by the diamagnetic contributions of the phases which are present in the phase mixtures as well as by contribution stemming from the gelatin capsule and straw used for sample mounting. [16] Since no deviations between the FC and ZFC measurements were observed, only the ZFC data are shown.

2.8 X-Ray Photoelectron Spectroscopy

The surface oxidation states of Ti were examined by XPS analysis on a Physical Electronic VersaProbe XPS unit (PHI 5000 spectrometer) with Al Kα radiation (1486.6 eV). All detail spectra were recorded at an electron escape angle of 75° with a step size of 0.1 eV, a pass energy of 23.5 eV and a spot diameter of 200 µm. A neutralizer was used for the compensation of surface charging.

Samples were transferred from an Ar-filled glovebox to the ultra-high-vacuum system of the spectrometer in Ar-atmosphere using a sealed transfer chamber capable of in vacuo transportation to minimize surface oxidation processes.

The binding energies of $Sr_3Ti_2O_5F_4$ were calibrated to the carbon 1s (C 1s) emission line at 284.8 eV. Due to the absence of carbon signals within the reacted mixtures $Sr_3Ti_2O_5F_4$ + x NaH with x = 2 and x = 4 and the formation of a surface layer of NaF on the reduced RP particles, the binding energies were calibrated to the sodium 1s (Na 1s) line at 1071.1 eV.

3 Results and Discussion

3.1 Topochemical Fluorination of $Sr_3Ti_2O_7$ to $Sr_3Ti_2O_5F_4$

3.1.1 Structural Analysis of $Sr_3Ti_2O_5F_4$

The precursor oxide $Sr_3Ti_2O_7$ crystallizes in the RP type structure with the tetragonal space group *I*4/*mmm* (a = 3.89890(15) Å and c = 20.3125(10) Å, $V_{f.u.}$ = 154.39(2) Å^3). [17]

The XRD patterns of $Sr_3Ti_2O_7$ and $Sr_3Ti_2O_5F_4$ are shown in Figure 1. The chemical fluorination of $Sr_3Ti_2O_7$ to $Sr_3Ti_2O_5F_4$ results in a significant cell expansion of ~ 15.8 % ($V_{f.u.}$ = 178.724(1) Å^3). This expansion is due to a strong expansion along the c-axis (~ 15.0 %), while the a- and b-axes remain almost constant (a = 3.9059(8) Å and c = 23.372(5) Å). In agreement with previously fluorinated n = 2 RP compounds with high filling degrees of the interstitial layers [18, 19], good refinements could be obtained within the parent space group of *I*4/*mmm*. Symmetry lowering is not indicated due to the absence of reflection splitting and superstructure reflections. Additionally, ~ 5 wt-% of SrF_2 and ~ 7 wt-% of $SrTiO_3$ are formed due to partial decomposition (due to variations in the levels of decomposition between samples, the amounts of SrF_2 and $SrTiO_3$ can vary slightly for different synthesis batches within this article). These impurity phases remain present in all defluorination products, and their relative phase fractions do not show strong changes within errors.

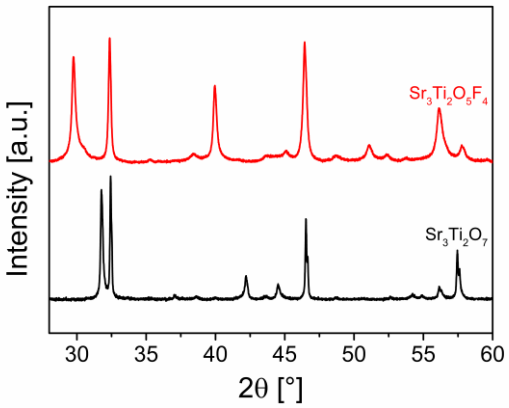

Figure 1: XRD patterns of $Sr_3Ti_2O_7$ and $Sr_3Ti_2O_5F_4$.

The structural refinement of $Sr_3Ti_2O_5F_4$ was performed via a coupled Rietveld analysis of XRD and NPD data (Figure 2). The obtained structural parameters and bond distances are given in Table 1 and

Table 2, respectively. The bond distances of $Sr_3Ti_2O_7$ are listed for comparison. For $Sr_3Ti_2O_5F_4$, it was found that all anion sites are fully occupied within errors, suggesting a composition of $Sr_3Ti_2X_9$ with X being oxide or fluoride because neither ion can be distinguished by powder diffraction methods. The diamagnetic nature of the sample after fluorination supports the presence of Ti^{4+} (see section 3.3.1), which is in good agreement with the assumed composition of $Sr_3Ti_2O_5F_4$.

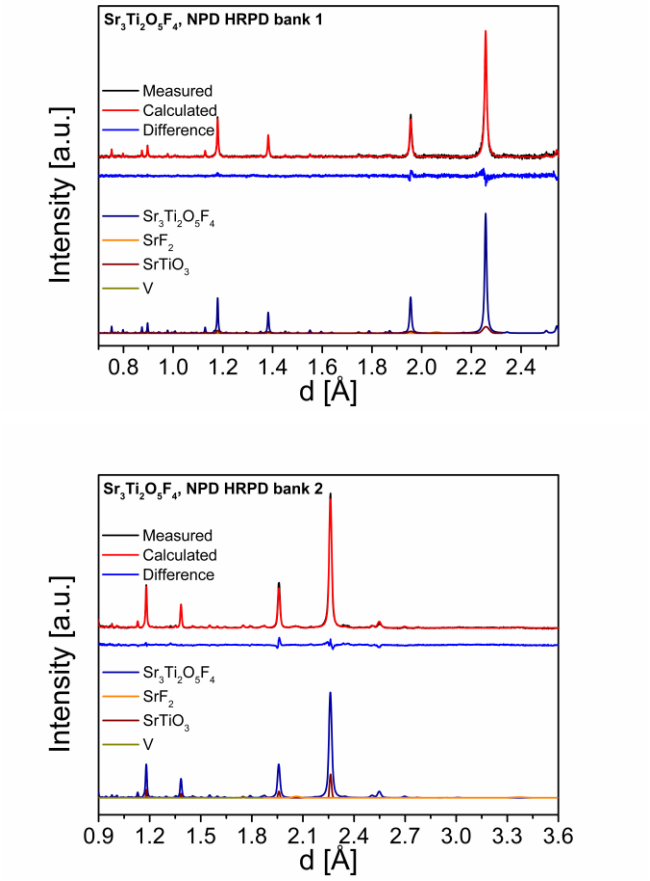
Sr3Ti2O5F4, NPD HRPD bank 1
Measured
Calculated
Difference
Sr3Ti2O5F4
SrF2
SrTiO3
V
Intensity [a.u.]
0.8 1.0 1.2 1.4 1.6 1.8 2.0 2.2 2.4
d [Å]
Sr3Ti2O5F4, NPD HRPD bank 2
Measured
Calculated
Difference
Sr3Ti2O5F4
SrF2
SrTiO3
V
Intensity [a.u.]
0.9 1.2 1.5 1.8 2.1 2.4 2.7 3.0 3.3 3.6
d [Å]

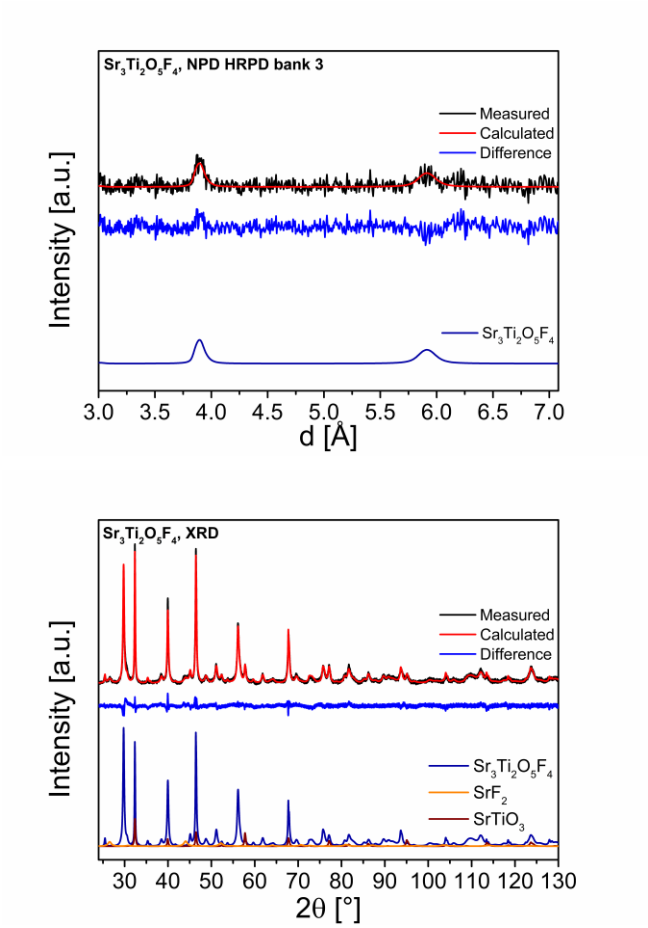

Figure 2: Coupled Rietveld analysis of $Sr_3Ti_2O_5F_4$ (space group: I4/mmm) of HRPD bank 1 data, HRPD bank 2 data , HRPD bank 3 data and XRD data.

Table 1: Structural parameters of $Sr_3Ti_2O_5F_4$ (space group: I4/mmm) from coupled Rietveld analysis of XRD and NPD data. The assignment of oxide and fluoride ions to different anion sites is based on DFT calculations.

Atom	**Wyckoff site**	**x**	**y**	**z**	**Occ.**	**B [Å^2]**
Sr1	2*b*	**0**	**0**	**½**	**1**	1.07(2)
Sr2	4*e*	**0**	**0**	0.31381(5)	**1**	1.07(2)
Ti1	4*e*	**0**	**0**	0.0804(1)	**1**	1.07(2)
O1 at X1 (equatorial site)	8*g*	**0**	**½**	0.0822(1)	**1**	1.07(2)
O2 at X2 (apical site (central))	2*a*	**0**	**0**	**0**	**1**	1.07(2)
F1 at X3 (apical site (terminal))	4*e*	**0**	**0**	0.8335(1)	**1**	1.07(2)
F2 at X4 (interlayer site)	4*d*	**½**	**0**	**¼**	**1**	1.07(2)

***a* [Å]**	3.9059(8)	***c* [Å]**	23.372(5)

R_{wp} (XRD+NPD) [%] 2.98	***GOF (XRD+NPD)*** 1.83	***R_{Bragg} [%]*** 0.98 (XRD) 2.75 (NPD, bank 1)

Table 2: Bond distances of $Sr_3Ti_2O_7$ and $Sr_3Ti_2O_5F_4$. Anion sites are referred to as X1 (= equatorial site), X2 (= apical site (central)), X3 (= apical site (terminal)) and X4 (= interlayer site).

	Bond distance [Å]	
Bond	**$Sr_3Ti_2O_7$**	**$Sr_3Ti_2O_5F_4$**
Sr1 – X1	2.755(3) [8x]	2.750(2) [8x]
Sr1 – X2	2.7572(1) [4x]	2.7723(3) [4x]
Sr2 – X1	2.674(3) [4x]	3.130(2) [4x]
Sr2 – X3	2.7593(2) [4x]	2.8105(6) [4x]
Sr2 – X4		2.4666(8) [4x]
Ti1 – X1	1.9501(1) [4x]	1.9608(4) [4x]
Ti1 – X2	1.989(2) [1x]	1.886(2) [1x]
Ti1 – X3	1.897(5) [1x]	2.020(3) [4x]

Bond valence sum (BVS) calculations have been used to assign the anions to their respective crystallographic sites. Different possible anion distribution models of oxide and fluoride ions have been tested and the results are listed in Table 3. The lowest global instability index (GII) and, therefore, the most stable configuration was found when fluoride ions are located at the interstitial site (X4) and the terminal apical site (X3). This is in good agreement with previous studies on Ruddlesden-Popper type compounds

[18], and similar to what was found previously for $Sr_2TiO_3F_2$. [6] The refined crystal structure of $Sr_3Ti_2O_5F_4$ with the most stable anion configuration is given in Figure 3.

Table 3: Results of bond valence sum calculations for $Sr_3Ti_2O_5F_4$ for different O/F distributions on anion sites. Anion sites are referred to as X1 (= equatorial site), X2 (= apical site (central)), X3 (= apical site (terminal)) and X4 (= interlayer site). Mixed occupancies of sites were also considered.

Arrangement of oxide and ions and anion sites X1, X2, X3 and X4	**Bond valance sum**	**Global instability index (GII)**
$O1_{X1} – O2_{X2} – F1_{X3} – F2_{X4}$	O1: 2.0482 O2: 1.6843 F1: 0.9924 F2: 1.1048	0.2541
$O1_{X1} – F1_{X2} – O2_{X3} – O3_{X4}$	O1: 2.0482 O2: 1.3438 O3: 1.1801 F1: 1.4388	0.4811
$O1_{X1} – 0.5O2/0.5F2_{X2} – O3_{X3} – F1_{X4}$	O1: 2.0482 O2: 1.6843 F2: 1.1048 O3: 1.1801 F1: 1.4388	0.3981
$F1_{X1} – O2_{X2} – 0.5O3/0.5F3_{X3} – F3_{X4}$	F1: 1.7471 O2: 1.6843 O3: 1.1801 F2: 0.9924 F3: 1.1048	0.4095
$O1_{X1} – 0.5O2/0.5F2_{X2} – F3_{X3} – O3_{X4}$	F1: 2.0482 O2: 1.6843 F2: 1.4388 F3: 0.9942 O4: 1.3471	0.3575
$F_{X1} – 0.75O2/0.25F2_{X2} – O3_{X3} – F1_{X4}$	F1: 1.7471 O2: 1.6843 F2: 1.4388 O3: 1.1801 F1: 1.1048	0.4342
$F1_{X1} – 0.25O2/0.75F2_{X2} – O3_{X3} – O4_{X4}$	F1: 1.7471 O2: 1.6843 F2: 1.4388 O3: 1.1801 O4: 1.3438	0.4839

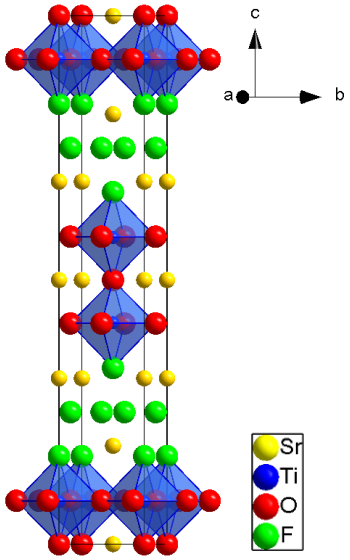

Figure 3: Crystal structure of $Sr_3Ti_2O_5F_4$ for an $O1_{X1} – O2_{X2} – F1_{X3} – F2_{X4}$ arrangement of anion sites based on BVS calculations. Anion sites are referred to as X1 (= equatorial site), X2 (= apical site (central)), X3 (= apical site (terminal)) and X4 (= interlayer site).

3.2 Topochemical Reduction of $Sr_3Ti_2O_5F_4$

3.2.1 Analysis of Reduction Mechanism

To study the behavior of $Sr_3Ti_2O_5F_4$ on the reductive deintercalation of fluoride ions, defluorination reactions between various mixtures of $Sr_3Ti_2O_5F_4$ + x NaH with $0.5 \leq x \leq 4$ have been performed. The X-ray diffraction data show a complex behavior illustrating the formation of various RP type reaction products (Figure 4), which were quantitatively evaluated using the Rietveld method (see Electronic Supplementary Table S1 for a detailed summary of refined lattice parameters, phase contents and unit cell volumes). It was found that none of the patterns can be sufficiently accurately described using a single RP type phase or one with lowered symmetry. Due to the broad range of compositions studied, suitable compositions could be determined, for which an individual phase is predominant. These phases were additionally studied with neutron diffraction to determine suitable structural models (see section 3.2.2). In summary, five different phases could be identified, namely four tetragonal phases (space group *I*4/*mmm*) and one orthorhombic phase (space group *Fmmm*). The evolution of the weight fractions of the different phases is depicted in Figure 5 a).

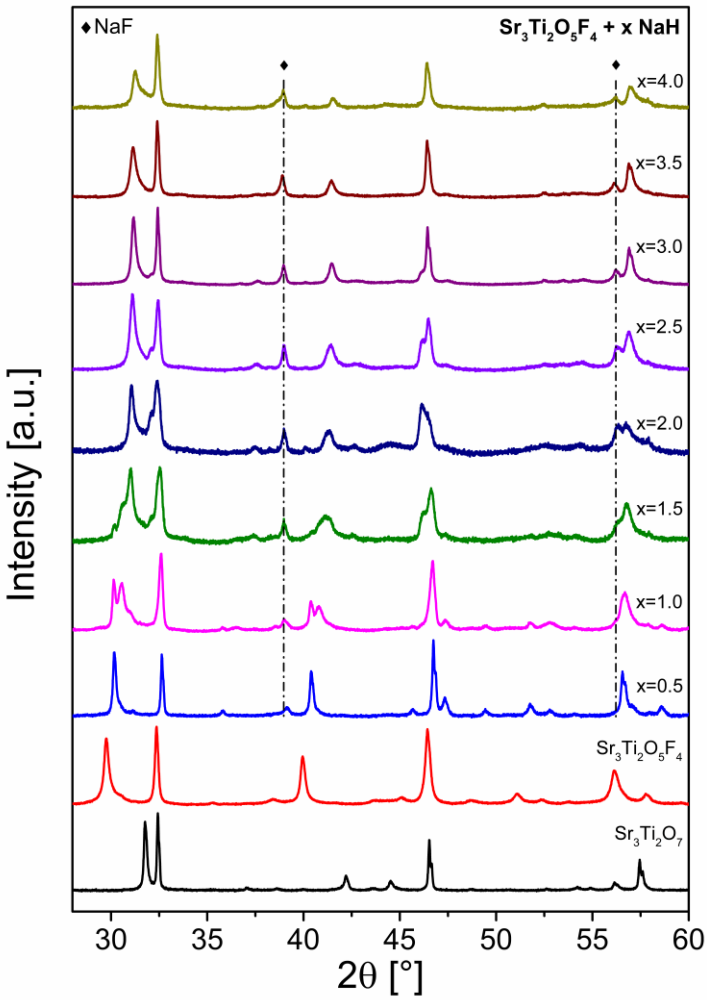

Figure 4: X-ray diffraction patterns of $Sr_3Ti_2O_7$, $Sr_3Ti_2O_5F_4$ and reduction reaction products $Sr_3Ti_2O_5F_4$ + x NaH ($0.5 \leq x \leq 4$) containing reduced RP type phases $Sr_3Ti_2O_5F_{4-x}H_y$. For the Rietveld refinements of the patterns shown together with an assignment of reflections to $Sr_3Ti_2O_7$, $Sr_3Ti_2O_5F_4$, the reduced phases and the side products (SrF_2, $SrTiO_3$, NaF, $NaF_{1-z}H_z$) the reader is referred to Figure S 1 in the Electronic Supplementary.

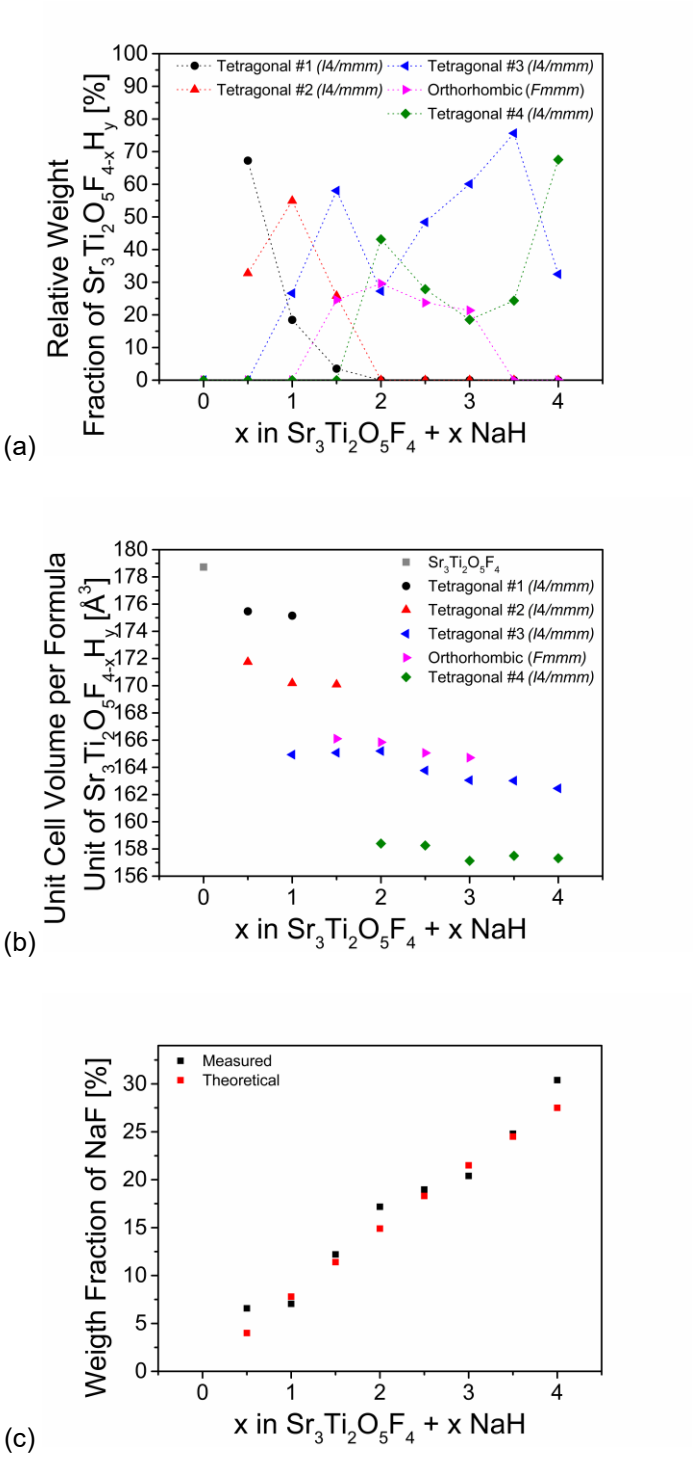

Figure 5: (a) Relative weight fractions of reduced RP type phases $Sr_3Ti_2O_5F_{4-x}H_y$ in the reduction reaction products $Sr_3Ti_2O_5F_4$ + x NaH ($0.5 \leq x \leq 4$), not considering further phases such as NaF, $NaF_{1-z}H_z$, $SrTiO_3$ and SrF_2 as a function of x; (b) Unit cell volumes per formula unit of $Sr_3Ti_2O_5F_4$ and reduced RP type phases $Sr_3Ti_2O_5F_{4-x}H_y$ as a function of x; (c) Weight fraction of NaF in reduction reaction products $Sr_3Ti_2O_5F_4$ + x NaH ($0.5 \leq x \leq 4$) as a function of x, together with theoretically expected values calculated from the amount of NaH added assuming full conversion to NaF.

In comparison to the parent oxyfluoride $Sr_3Ti_2O_5F_4$, strong shifts of reflections (*hkl*) with $I \neq 0$ can be observed for all reduced phases due to strong decreases of the *c* lattice parameters. These decreases lead to considerable unit cell volume changes (Figure 5 b). Higher amounts of added NaH result in higher reductions in the cell volumes. When considering a particular phase, the unit cell volume stays relatively constant, although smaller changes of lattice parameter indicate some degree of compositional flexibility for each phase. Smaller changes are also observed for lattice parameters *a* and *b,* which undergo a comparatively small expansion. This expansion within the a/b-plane originates from the formation of low-valent Ti species, which are larger than Ti^{4+}. [20]

On increasing the amount of reductant, a stronger degree of disorder is also introduced into the RP type structures. This can best be seen considering reflections (*hkl*) with $I \neq 0$ of the tetragonal #3 and #4 phases, which show significantly increased anisotropic broadening. This broadening is commonly observed for the reduction of RP type compounds [21], indicating the flexibility of the lattice to adopt compositional variations in a broader range. This also implies that the phases obtained for lower values of x, i.e. the tetragonal #1 and #2 as well as the orthorhombic phase, are highly ordered.

After the reactions, NaF (Figure 5 c) is present in all reaction products, and the degree of defluorination can be easily verified by comparing the weight fractions of measured NaF with the theoretically predicted amounts of NaF (i.e. the amount which would be expected assuming that all used NaH converts to NaF since no other source of fluoride is available). This also confirms that the multi-phase model, which has been used to describe the reflections of the RP phases gives an excellent approximation of the relative amount of each single phase fraction. Further, it indicates a negligible degree of decomposition on the reduction showing the stability of the phases upon defluorination (in contrast to Ni based oxyfluorides [22]). Small amounts of unreacted NaH form a mixed crystal $NaF_{1-z}H_z$ with NaF that can be identified as a shoulder next to all NaF reflections, and which increase for larger values of x. When looking at SEM images of $Sr_3Ti_2O_5F_4$ and the reduced products (Figure 6), it appears that the particles of the reduced samples have less smooth surfaces as compared to $Sr_3Ti_2O_5F_4$. Due to very high Na and F signals in the surface-sensitive XPS measurements (see section 3.3.2) it is indicated that NaF forms a layer of smaller particles on top of the reduced particles.

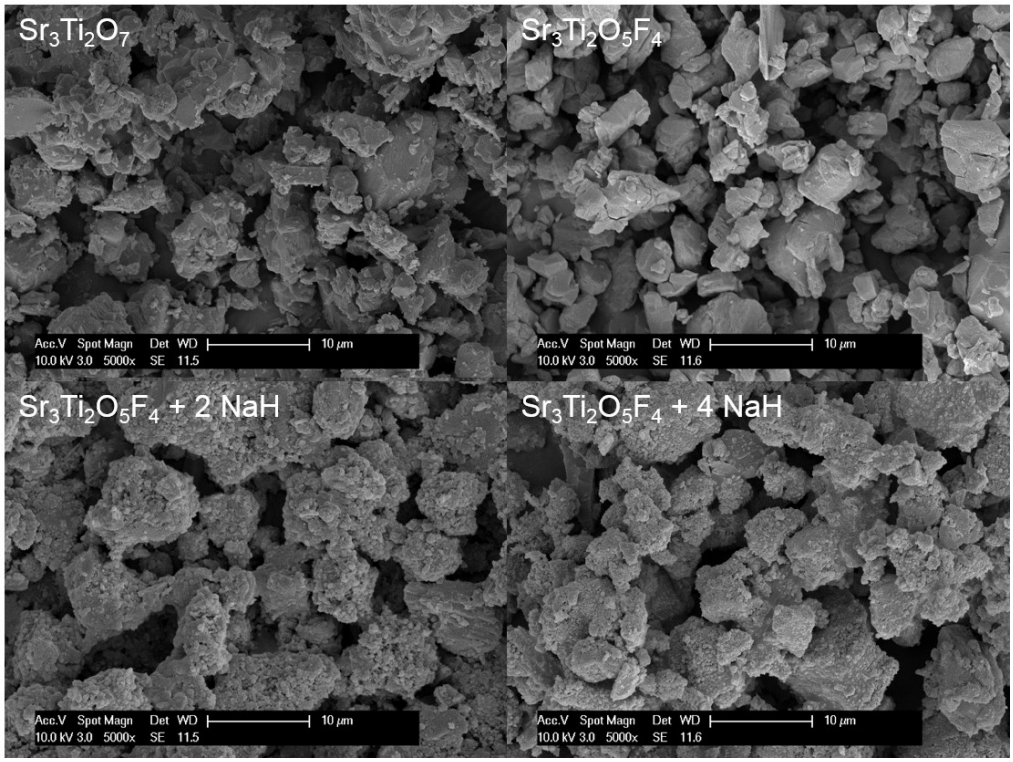

Figure 6: Scanning electron micrographs of $Sr_3Ti_2O_7$, $Sr_3Ti_2O_5F_4$ and the reduction reaction products $Sr_3Ti_2O_5F_4$ + x NaH with x = 2 and x = 4.

At this point, it is also worth emphasizing that the reduction behavior of the n = 2 RP type $Sr_3Ti_2O_5F_4$ with formation of different coexisting phases is different to what was observed previously on the reduction of the n = 1 RP type $Sr_2TiO_3F_2$.[6] There, relatively pure single-phase compounds could be isolated for the addition of 1 and 2 equivalents of NaH.

Elemental analysis confirms the presence of hydride ions within the reaction products, from which the formation of compounds with compositions of formally $Sr_3Ti_2O_5F_2H_{0.42(2)}$ + 2 NaF for x = 2 and $Sr_3Ti_2O_5H_{1.26(10)}$ + 4 NaF for x = 4 can be derived. Assuming a linear relationship between the hydride content and the lattice parameters ($a_{NaF} \approx 4.63$ Å [23], $a_{NaH} \approx 4.89$ Å [24]) of the partially formed $NaF_{1-z}H_z$ phases, an estimation of their hydride content is possible (see section Electronic Supplementary Table S 1). Taking also their phase fractions into account, it can be followed that only a small amount of the hydride ions contained in the reaction products is located in the $NaF_{1-z}H_z$ phase. Moreover, the presence of other hydride-containing side and decomposition products or substantial amorphization leading to the formation of amorphous hydride-containing products can be ruled out. Therefore, the most plausible host for a major part of the hydride ions are the reduced RP phases. Furthermore, the reduction of RP oxides using metal hydrides as reducing agent results commonly in the formation of oxyhydrides, e.g. the reaction between $Sr_3Ti_2O_7$ and CaH_2 at 480 °C leads to $Sr_3Ti_2O_{6.20(5)}H_{0.12(4)}$ [25]. Therefore, the formation of RP type oxide hydride fluorides is the most plausible explanation within this study. However, since two-phase mixtures of RP type oxyfluoride hydrides are found for values of x = 2 and x = 4, the exact hydride content of each individual RP type phase cannot be determined.

Regardless of this, the overall degree of fluoride-hydride substitution in comparison to the reductive defluorination under formation of H_2 is lower compared to previously reported $Sr_2TiO_3FH_{0.48(1)}$ (x = 1) and $Sr_2TiO_3H_{1.48(10)}$ (x = 2).[6] For the reduction of both the n = 1 and n = 2 oxyfluorides, the reductive defluorination is the predominant reaction mechanism for low NaH equivalents, and fluoride-hydride exchange becomes dominant for increasing amounts of NaH.

Re-oxidation experiments on $Sr_3Ti_2O_5F_4$ + x NaH (x = 2 and x = 4) were performed, which can also serve to confirm the successful defluorination. On exposure of the compounds to air at elevated temperatures, phase mixtures containing several re-oxidized phases of $Sr_3Ti_2O_{5+x/2}F_{2-x}$ with varying values of x as well as side and decomposition products (NaF, increased amounts of $SrTiO_3$, TiO_2 and SrF_2) are found (see Electronic Supplementary Figure S 2 and Table S 2). The lattice parameters of the re-oxidized phases have *c* lattice parameters between those of $Sr_3Ti_2O_7$ and $Sr_3Ti_2O_5F_4$, showing that a certain oxide-fluoride disorder is present in the phases. The fact that $Sr_3Ti_2O_7$ is not formed on re-oxidation suggests that a complete defluorination of $Sr_3Ti_2O_5F_4$ to $Sr_3Ti_2O_5$ has not taken place for the highest amount of NaH added, in agreement with the observation of $NaF_{1-z}H_z$. However, the phase fractions of the phases with smaller *c* lattice parameters increase considerably when the re-oxidation is performed on the more strongly reduced phases, which contain less fluoride. Overall, the phase fractions and the lattice parameters of the re-oxidized oxyfluorides are in good agreement with the assumed degree of defluorination.

3.2.2 Structural Analyses of Defluorination Products

Structural analyses of the reaction products $Sr_3Ti_2O_5F_4$ + x NaH with x = 2 and x = 4 were performed via coupled analysis of XRD and NPD data. The refined patterns of $Sr_3Ti_2O_5F_4$ + 2 NaH and $Sr_3Ti_2O_5F_4$ + 4 NaH are shown in Figure 7 and Figure S 3 in the Electronic Supplementary, respectively.

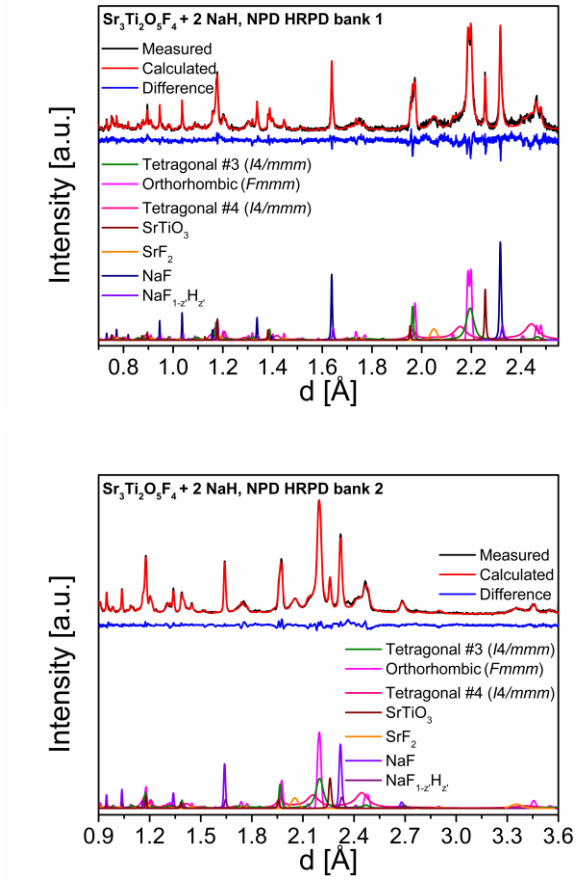
Sr3Ti2O5F4 + 2 NaH, NPD HRPD bank 1
Measured
Calculated
Difference
Tetragonal #3 (I4/mmm)
Orthorhombic (Fmmm)
Tetragonal #4 (I4/mmm)
SrTiO3
SrF2
NaF
NaF1-zHz
Intensity [a.u.]
0.8 1.0 1.2 1.4 1.6 1.8 2.0 2.2 2.4
d [Å]
Sr3Ti2O5F4 + 2 NaH, NPD HRPD bank 2
Measured
Calculated
Difference
Tetragonal #3 (I4/mmm)
Orthorhombic (Fmmm)
Tetragonal #4 (I4/mmm)
SrTiO3
SrF2
NaF
NaF1-zHz
Intensity [a.u.]
0.9 1.2 1.5 1.8 2.1 2.4 2.7 3.0 3.3 3.6
d [Å]

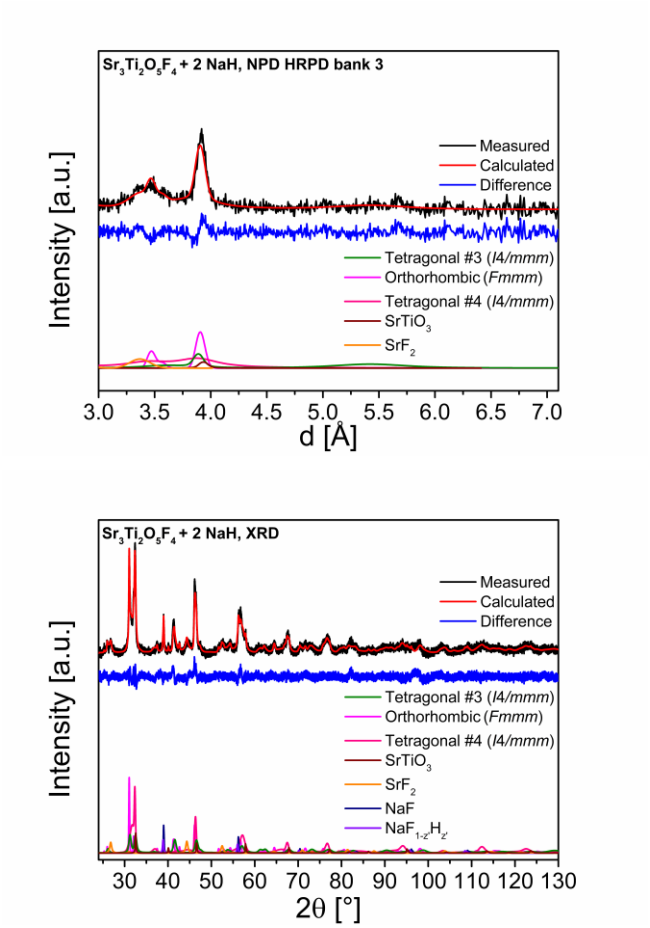

Figure 7: Coupled Rietveld analysis of reduction reaction products $Sr_3Ti_2O_5F_4$ + 2 NaH containing reduced RP type phases $Sr_3Ti_2O_5F_{4-x}H_y$ of HRPD bank 1 data, HRPD bank 2 data, HRPD bank 3 data and XRD data.

In $Sr_3Ti_2O_5F_4$ + 2 NaH, three RP type phases, i.e. two tetragonal phases (called tetragonal #3 and #4) and an orthorhombic phase are found. The highest phase fraction of the latter phase across the whole series is found within this reaction product. In $Sr_3Ti_2O_5F_4$ + 4 NaH, only the tetragonal phases #3 and #4 are present. Since only multi-phase mixtures were obtained within this study, which is in clear contrast to our previous study on the reduction of $Sr_2TiO_3F_2$, it is not possible to assign an unambiguous anion composition to each phase. Moreover, it is also not possible to distinguish between hydride and oxide/fluoride ions on sites, which contain anion vacancies in addition. This is related to the fact that the anion substructure is mainly determined from the neutron diffraction data of the coupled analysis and by the scattering lengths of the different species (^{1}H: -3.7 fm, ^{16}O: 5.8 fm, ^{19}F: 5.7 fm). As a simple example, having a site occupied partly by oxide ions and vacancies, or having it occupied by slightly more oxide ions, a small amount of hydride ions and a lower amount of vacancies would provide equal mathematics within the neutron analysis, at the cost of a higher amount of refinement parameters. Therefore, occupation factors of the reported structures are given as occupancies of oxide and/or fluoride ions only. This, however, also implies that, if vacancies are present on a certain site, hydride ions can be present on the same site with the same validity.

A very detailed structural analysis on the tetragonal phases is not possible due to a strong correlation of the parameters. The intensity patterns can be accurately described with structural models of the aristotype RP n = 2 structure with *I4/mmm* symmetry. The analysis of this phase, especially of the tetragonal #4 phase, is further impeded by strong anistropic reflection broadening, which can be fitted with the aid of a Stephen's model. [26] This is indicative for the presence of a distribution of multiple phases with slightly varying *c* lattice parameters. Regardless of these implications, the structural refinements indicate that considerable amounts of vacancies are present on the interlayer site of both phases and on the apical (terminal) anion site of the tetragonal phase #4. Moreover, decreasing occupation factors of these sites in $Sr_3Ti_2O_5F_4$ + x NaH with x = 4 as compared to x = 2 are plausible considering that higher degrees of defluorination should be expected when using higher NaH amounts. Structural parameters of the tetragonal #3 phase are given in the Electronic Supplementary Table S 3.

For the patterns of $Sr_3Ti_2O_5F_4$ + 2 NaH, some of the sharper reflections (e.g. $(110)_{I4/mmm}$ or $(116)_{I4/mmm}$) show reflection splitting suggesting the presence of a phase, which has undergone a symmetry lowering to orthorhombic symmetry. A model within the translationengleiche supgroup *Fmmm* with a cell size of $\sqrt{2}$ x $\sqrt{2}$ x 1 of the aristotype structure allows for a good fitting of the positions of the reflections. Further loss of translational symmetry can be excluded due to the absence of superstructure reflections. The neutron diffraction data can, moreover, give valuable information about the approximate structure and composition of the anion sublattice, since, while oxide and fluoride cannot be distinguished from each other, they can be differentiated from anion vacancies. The equatorial and the apical (central) sites are found to be fully occupied by oxide and/or fluoride within errors and their occupations have, therefore, been fixed to 100 %. The occupation factors of the apical (terminal) and the interlayer sites, on the other hand, are significantly decreased due to the extraction of fluoride upon defluorination resulting in a formal composition of the orthorhombic phase of $Sr_3Ti_2O_5F_{1.86}H_y$. The refined structural parameters and bond distances are given in Table 4 and Table 5, respectively. The crystal structure of the orthorhombic phase is shown in Figure 8. The assignment of the oxide and fluoride to the different anion sites was done based on the most stable anion configuration of $Sr_3Ti_2O_5F_4$ (see section 3.1.1) supported by the fact that, due to fluoride extraction, only the apical (terminal) and interlayer anion sites are not fully occupied.

Table 4: Structural parameters of the orthorhombic phase $Sr_3Ti_2O_5F_{1.86}H_y$ (space group: Fmmm) from coupled Rietveld analysis of XRD and NPD data of $Sr_3Ti_2O_5F_4$ + 2 NaH.

Atom	**Wyckoff site**	**x**	**y**	**z**	**Occ.**	**B [Å^2]**
Sr1	4*b*	**0**	**0**	**½**	**1**	0.87(6)
Sr2	8*i*	**0**	**0**	0.6818(2)	**1**	0.87(6)
Ti1	8*i*	**0**	**0**	0.9147(4)	**1**	0.87(6)
O1 at X1 (equatorial site)	16*j*	**¼**	**¼**	0.4024(2)	**1**	0.87(6)
O2 at X2 (apical site (central))	4*a*	**0**	**0**	**0**	**1**	0.87(6)
F1 at X3 (apical site (terminal))	8*i*	**0**	**0**	0.1721(9)	0.30(1)	0.87(6)
F2 at X4 (interlayer site)	8*f*	¼	¼	¼	0.63(2)	0.87(6)

***a* [Å]**	5.6083(4)	***b* [Å]**	5.5596(9)	***c* [Å]**	21.275(3)
R_{wp} **(XRD+NPD) [%]** 3.09		***GOF (XRD+NPD)*** 1.71		R_{Bragg} **[%]** 0.99 (XRD) 3.61 (NPD, bank 1)	

Table 5: Bond distances of orthorhombic phase $Sr_3Ti_2O_5F_{1.86}H_y$ (space group: Fmmm). Anion sites are referred to as X1 (= equatorial site), X2 (= apical site (central)), X3 (= apical site (terminal)) and X4 (= interlayer site).

	Bond distance [Å]
Bond	**$Sr_3Ti_2O_5F_{1.86}H_y$**
Sr1 – X1	2.865(3) [8x]
Sr1 – X2	2.8042(2) [4x]
Sr2 – X1	2.666(4) [4x]
Sr2 – X3	2.787(2) [2x] 2.812(2) [2x]
Sr2 – X4	2.450(3) [4x]
Ti1 – X1	1.992(1) [4x]
Ti1 – X2	1.815(9) [1x]
Ti1 – X3	1.847(2) [1x]

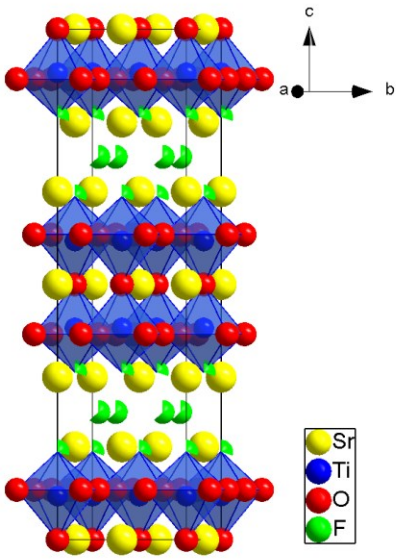

Figure 8: Crystal structure of the orthorhombic phase $Sr_3Ti_2O_5F_{1.86}H_y$ (space group: Fmmm) for an $O1_{X1} – O2_{X2} – F1_{X3} – F2_{X4}$ arrangement of anion sites. Anion sites are referred to as X1 (= equatorial site), X2 (= apical site (central)), X3 (= apical site (terminal)) and X4 (= interlayer site).

3.3 Determination of Ti oxidation states

3.3.1 Magnetization Study

The ZFC M(T) curves of $Sr_3Ti_2O_5F_4$ and reduction reaction products $Sr_3Ti_2O_5F_4$ + x NaH with x = 2 and x = 4, respectively, are shown in Figure 9. $Sr_3Ti_2O_5F_4$ behaves diamagnetically in the whole temperature range. This is due to the presence of diamagnetic Ti^{4+} cations with d^0 configuration only. In contrast to this, the reduced compounds show predominantly paramagnetic behavior reflecting the presence of unpaired electrons and, thus, confirming a successful defluorination and reduction of the Ti oxidation state. Different Curie-Weiss law related fitting strategies have been previously used in literature to describe the temperature dependence of the magnetization of reduced titanates. No linear behaviour of the $1/\chi(T)$ curves (Figure 9) could be observe. Blundred al. [27] could also not observe such a linear behavior of $1/\chi(T)$ for reduced pyrochlore $Lu_2Ti_2O_{6.10}$ over the whole temperature range and used only a limited temperature range between 200 and 300 K, i.e. where ideal paramagnetic behavior should be more dominant. Using this simple model to the reaction products with x = 2 and x = 4, still no perfect linear behavior of $1/\chi(T)$ (see Electronic Supplementary Figure S 4 a) could be observed in the high-temperature range of 100 to 250 K, even though the measurements were corrected from diamagnetic contributions of the present phases and the gelatin capsules and straws used during the measurements [16]. A modified Curie-Weiss model according to $\chi = C/(T - \Theta) + \chi_0$ where χ_0 is a temperature-independent term to assign for deviations from ideal paramagnetism was applied by Pussacq et al. [28] over an extended temperature range to take diamagnetic and ferromagnetic contributions originating from the reduction of $La_2Ti_2O_7$ into account. For the reaction products with x = 2 and x = 4, the modified Curie-Weiss law over the whole temperature range resulted, however, in insufficient

description of the recorded data (see Electronic Supplementary Figure S 4 b). These deviations from Curie-Weiss behavior suggest that the reduction reaction products are not ideally paramagnetic and that the magnetic moments obtained (ranging from ~ 0.2 (modified Curie-Weiss fit) to ~1.4 μ_B per Ti atom (Curie-Weiss fit at higher temperatures) (see Electronic Supplementary Table S 4 for fitting parameters and obtained moments) cannot be interpreted unambiguously as being spin-only moments from low-valent Ti species; nevertheless, their order of magnitude is very similar to what was observed in the previous studies with the respective different fit models [27, 28].

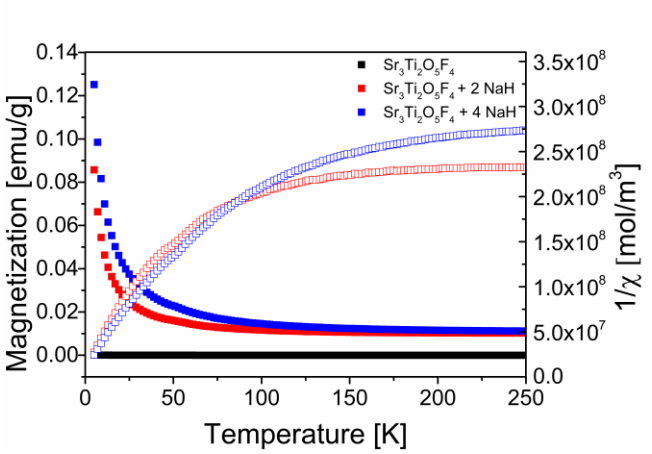

Figure 9: M(T) curves of $Sr_3Ti_2O_5F_4$ and reduction reaction products $Sr_3Ti_2O_5F_4$ + x NaH with x = 2 and x = 4 (filled symbols), 1/χ(t) curves of reduction reaction products $Sr_3Ti_2O_5F_4$ + x NaH with x = 2 and x = 4 (open symbols). The data were corrected by the diamagnetic contributions of the present phases and the gelatin capsules and straws used.

3.3.2 X-Ray Photoelectron Spectroscopy

Surface sensitive XPS measurements of $Sr_3Ti_2O_5F_4$ and the reduction reaction products $Sr_3Ti_2O_5F_4$ + x NaH with x = 2 and x = 4 allow the possibility to draw conclusions about the Ti oxidation states on the surface of the particles. The Ti $2p_{3/2}$ spectra are given in Figure 10. The poor signal-to-noise ratio of the Ti $2p_{3/2}$ spectra of the reduction products in comparison to the spectrum of $Sr_3Ti_2O_5F_4$ is due to a layer of NaF, which is formed upon defluorination on the surface of the particles of the RP phases. The presence of this layer can be confirmed by the high intensity of the Na 1s and F 1s spectra (see Figure S 5 in the Electronic Supplementary), which is also in agreement with the SEM images (Figure 6).

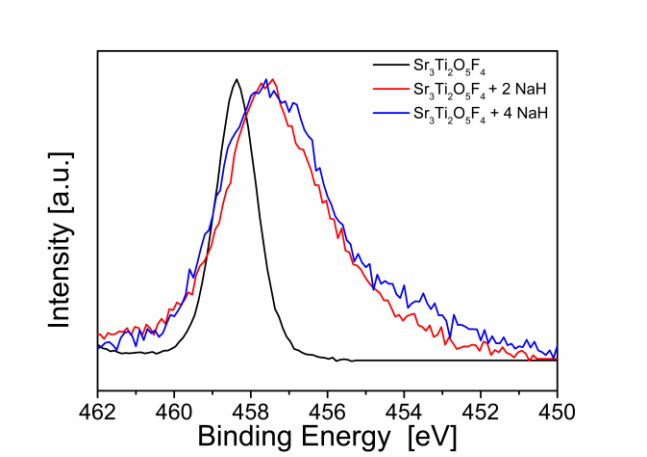

Figure 10: Normalized Ti $2p_{3/2}$ XPS spectra of $Sr_3Ti_2O_5F_4$ and reduction reaction products $Sr_3Ti_2O_5F_4$ + x NaH with x = 2 and x = 4.

The spectrum of $Sr_3Ti_2O_5F_4$ features a peak at ~ 458.4 eV with a FWHM of ~ 1.25 eV, which is typical for Ti^{4+} and suggests the existence of this oxidation state only. [29] In the spectra of the reduced compounds, considerable shifts towards lower binding energies and broader signals are observed. Characteristic binding energies of Ti^{3+} and Ti^{2+} containing oxides have been reported at ~ 457.7 eV and ~ 454.7 eV [30], respectively, corresponding well to the found signals. Therefore, it can be concluded that a strong reduction with the co-existence of different oxidation states has taken place on the surface of the particles of the RP phases. A precise quantification of the intensities of the different signals is hindered by the poor quality of the spectra. However, the strongest reduction seems to have occurred in $Sr_3Ti_2O_5F_4$ + 4 NaH, which is indicated by the extended tail to lower binding energies.

3.4 Comparison between Reduction of n = 1 and n = 2 Ruddlesden-Popper type Strontium Titanate Compounds

At this point a comparison between the phases obtained via chemical reduction of the RP type compounds $Sr_3Ti_2O_5F_4$ with n = 2 and $Sr_2TiO_3F_2$ with n = 1 [6] is interesting. For both parent oxyfluorides, considerable cell volume reductions, primarily due to decreases in the *c* lattice parameters of the reduced phases, are observed. In both cases, depending on the amount of NaH used, phases with reduced symmetry (medium amounts of NaH) or with strong anisotropic strain broadening (high amounts of NaH) are obtained. While for the reduction of the n = 1 compound nearly single-phase reaction products have been obtained for certain values of x, the reduction products of the n = 2 compound contain multi-phase mixtures independent on the amount of reducing agent. This indicates that the reduction of the n = 2 compound is more complex with either a variety of phases of similar stability or limited reaction kinetics avoiding the compositional equilibration of products.

The fluoride-hydride substitution is significantly less pronounced in the n = 2 compound resulting also in lower observed oxidation states. On the particle surfaces, strong reductions with Ti oxidation states as low as +2 are observed. An extended release of hydride on the particle surface, as observed for the n = 1 compounds, can, however, not be confirmed for the n = 2 compounds by XPS measurements. This might

be related to the different overall amounts of NaH that need to be used for the reaction, which might result in different degrees of surface covering of the particles by NaF. This covering might act as a diffusion barrier for the release of surface H_2; however, further studies would be clearly required to confirm this hypothesis.

4 Conclusions

Within this study, it was shown that the topochemical fluorination of $Sr_3Ti_2O_7$ to $Sr_3Ti_2O_5F_4$ using the fluorine-containing polymer PVDF results in the insertion of two fluoride ions into the interstitial sites and substitution of two oxide ions on the terminal apical site by two fluoride ions.

The selective topochemical defluorination of $Sr_3Ti_2O_5F_4$ leads to considerable reduction and the formation of low-valent Ti species. Reactions have been performed according to the reaction equation $Sr_3Ti_2O_5F_4$ + x NaH ($0.5 \leq x \leq 4$). As a function of the amount of reducing agent NaH, complex phase mixtures containing several different strongly reduced phases could be identified and structural changes were investigated. The phase $Sr_3Ti_2O_5F_{1.86}H_y$ has been found for $1.5 \leq x \leq 3$, for which a symmetry lowering from *I*4/*mmm* to *Fmmm* could be confirmed by a coupled Rietveld analysis of X-ray and neutron powder diffraction data. For even higher degrees of defluorination, phases with strong anisotropic broadening have been observed. The formation of low-valent Ti has been confirmed by magnetic and XPS measurements. Overall, the phase formation behavior is more complex compared to what was observed for the reduction of $Sr_2TiO_3F_2$, for which compositions closer to single-phase products could be observed. [6]

Further, the chosen sequence of topochemical reactions involving the fluorination via combined fluoride insertion and partial oxide-fluoride exchange, followed by the reductive defluorination under partial fluoride-hydride exchange can be considered as a complementary route for the formation of oxide fluoride hydrides as compared to a method previously suggested by Masuda et al. [3] In their work, the synthesis of $BaTi(O,H,F)_3$ is achieved using a hydride-based topochemical reduction, which causes an oxide-hydride exchange, followed by a NH_4F-based fluorination, which leads to a hydride-fluoride exchange. Therefore, in terms of anion exchange reactions, these routes can be regarded as reversed approaches.

5 Associated Contents / Supporting paragraphs

The Supporting Information is available free of charge on the ACS Publications website at DOI: xxx.

Quantitative analysis and refined lattice parameters and unit cell volumes of XRD data of $Sr_3Ti_2O_5F_4$, reduction reaction products $Sr_3Ti_2O_5F_4$ + x NaH ($0.5 \leq x \leq 4$) and of re-oxidized reduction reaction products; Rietveld refinements of $Sr_3Ti_2O_7$, $Sr_3Ti_2O_5F_4$, reduction reaction products $Sr_3Ti_2O_5F_4$ + x NaH ($0.5 \leq x \leq 4$) and of re-oxidized reduction reaction products; structural parameters of the tetragonal #3 phase; Curie-Weiss fits, fitting parameters and magnetic moments of reduction reaction products $Sr_3Ti_2O_5F_4$ + x NaH with x = 2 and x = 4; XPS spectra of $Sr_3Ti_2O_5F_4$ and reduction reaction products $Sr_3Ti_2O_5F_4$ + x NaH with x = 2 and x = 4.

Accession Codes CCDC 1952627 and 1952628 contain the supplementary crystallographic data for this paper. These data can be obtained free of charge via www.ccdc.cam.ac.uk/data_request/cif, or by emailing data_ request@ccdc.cam.ac.uk, or by contacting The Cambridge Crystallographic Data Centre, 12 Union Road, Cambridge CB2 1EZ, UK; fax: +44 1223 336033.

6 Acknowledgements

This work was funded by the German Research Foundation within the Emmy Noether program (Grant No. CL 551/2-1). Neutron diffraction beamtime on HRPD at ISIS was provided by the Science and Technology Facilities Council (STFC) (No. 1720040).

7 References

1. Greaves, C.; Francesconi, M. G., Fluorine insertion in inorganic materials. *Curr. Opin. Solid State Mater. Sci.* **1998,** *3* (2), 132-136.
2. Clemens, O.; Slater, P. R., Topochemical modifications of mixed metal oxide compounds by low-temperature fluorination routes. *Rev. Inorg. Chem.* **2013,** *33* (2-3).
3. Slater, P.; Driscoll, L., Modification of Magnetic and Electronic Properties, in Particular Superconductivity, by Low Temperature Insertion of Fluorine into Oxides. *Progr Fluor Sci Ser* **2016,** *1*, 401-421.
4. McCabe, E. E.; Greaves, C., Review: Fluorine insertion reactions into pre-formed metal oxides. *J. Fluorine Chem.* **2007,** *128*, 448-458.
5. Clemens, O.; Rongeat, C.; Reddy, M. A.; Giehr, A.; Fichtner, M.; Hahn, H., Electrochemical fluorination of perovskite type $BaFeO_{2.5}$. *Dalton Trans* **2014,** *43* (42), 15771-8.
6. Wissel, K.; Dasgupta, S.; Benes, A.; Schoch, R.; Bauer, M.; Witte, R.; Fortes, A. D.; Erdem, E.; Rohrer, J.; Clemens, O., Developing intercalation based anode materials for fluoride-ion batteries: topochemical reduction of $Sr_2TiO_3F_2$ via a hydride based defluorination process. *Journal of Materials Chemistry A* **2018,** *6* (44), 22013-22026.
7. Liu, B.; Huang, Y. H.; Barzegar Bafrooei, H.; Song, K. X.; Li, L.; Chen, X. M., Effects of structural transition on microwave dielectric properties of $Sr_3(Ti_{1-x}Sn_x)_2O_7$ ceramics. *J. Eur. Ceram. Soc.* **2019,** *39* (15), 4794-4799.
8. Liu, B.; Huang, Y. H.; Song, K. X.; Li, L.; Chen, X. M., Structural evolution and microwave dielectric properties in $Sr_2(Ti_{1-x}Sn_x)O_4$ ceramics. *J. Eur. Ceram. Soc.* **2018,** *38* (11), 3833-3839.
9. Slater, P. R., Poly(vinylidene fluoride) as a reagent for the synthesis of K_2NiF_4-related inorganic oxide fluorides. *J. Fluorine Chem.* **2002,** *117* (1), 43-45.
10. Ibberson, R. M., Design and performance of the new supermirror guide on HRPD at ISIS. *Nuclear Instruments & Methods in Physics Research Section a-Accelerators Spectrometers Detectors and Associated Equipment* **2009,** *600* (1), 47-49.
11. Ibberson, R. M. D., W.I.F.; Knight, K.S., The high resolution powder diffractometer (HRPD) at ISIS - a user guide. **1992**, DOI.
12. Arnold, O.; Bilheux, J. C.; Borreguero, J. M.; Buts, A.; Campbell, S. I.; Chapon, L.; Doucet, M.; Draper, N.; Ferraz Leal, R.; Gigg, M. A.; Lynch, V. E.; Markvardsen, A.; Mikkelson, D. J.; Mikkelson, R. L.; Miller, R.; Palmen, K.; Parker, P.; Passos, G.; Perring, T. G.; Peterson, P. F.; Ren, S.; Reuter, M. A.; Savici, A. T.; Taylor, J. W.; Taylor, R. J.; Tolchenov, R.; Zhou, W.; Zikovsky, J., Mantid—Data analysis and visualization package for neutron scattering and μ SR experiments. *Nuclear Instruments and Methods in Physics Research Section A: Accelerators, Spectrometers, Detectors and Associated Equipment* **2014,** *764* (Supplement C), 156-166.
13. *Topas V5, General profile and structure analysis software for powder diffraction data, User's Manual*. Bruker AXS: Karlsruhe, Germany, 2014, DOI.
14. Coelho, A. A. TOPAS-Academic. http://www.topas-academic.net (accessed 20th of October 2014).
15. Cheary, R. W.; Coelho, A. A.; Cline, J. P., Fundamental Parameters Line Profile Fitting in Laboratory Diffractometers. *J Res Natl Inst Stand Technol* **2004,** *109* (1), 1-25.

16. Bain, G. A.; Berry, J. F., Diamagnetic Corrections and Pascal's Constants. *J. Chem. Educ.* **2008,** *85* (4).
17. Ruddelson, S. N., Popper P. , The compund $Sr_3Ti_2O_7$ and its structure. *Acta Cryst.* **1958,** *11*, 54-55.
18. Gurusinghe, N. N.; Fones, J. C.; Marco, J. F.; Berry, F. J.; Greaves, C., Fluorine insertion into the Ruddlesden-Popper phase $La_2BaFe_2O_7$: the structure and magnetic properties of $La_2BaFe_2O_5F_4$. *Dalton Trans* **2014,** *43* (5), 2038-43.
19. Tsujimoto, Y.; Yamaura, K.; Hayashi, N.; Kodama, K.; Igawa, N.; Matsushita, Y.; Katsuya, Y.; Shirako, Y.; Akaogi, M.; Takayama-Muromachi, E., Topotactic Synthesis and Crystal Structure of a Highly Fluorinated Ruddlesden–Popper-Type Iron Oxide, $Sr_3Fe_2O_{5+x}F_{2-x}$ (x≈ 0.44). *Chem. Mater.* **2011,** *23* (16), 3652-3658.
20. Shannon, R. D., Revised Effective Ionic Radii and Systematic Studies of Interatomie Distances in Halides and Chaleogenides. *Acta. Cryst. A* **1976,** *32*, 751.
21. Kageyama, H.; Watanabe, T.; Tsujimoto, Y.; Kitada, A.; Sumida, Y.; Kanamori, K.; Yoshimura, K.; Hayashi, N.; Muranaka, S.; Takano, M.; Ceretti, M.; Paulus, W.; Ritter, C.; André, G., Spin-Ladder Iron Oxide: $Sr_3Fe_2O_5$. *Angew. Chem. Int. Ed.* **2008,** *47* (31), 5740-5745.
22. Wissel, K.; Malik, A. M.; Vasala, S.; Slater, P. R.; da Silva, I.; Alff, L.; Rohrer, J.; Clemens, O., Topochemical reduction of $La_2NiO_3F_2$: the first Ni-based Ruddlesden-Popper n = 1 T'-type structure and the impact of reduction on magnetic ordering. *submitted* **2019**, DOI.
23. Deshpande, V., Thermal expansion of sodium fluoride and sodium bromide. *Acta Crystallographica* **1961,** *14* (7), 794.
24. Shull, C. G.; Wollan, E. O.; Morton, G. A.; Davidson, W. L., Neutron Diffraction Studies of NaH and NaD. *Physical Review* **1948,** *73* (8), 842-847.
25. Hernandez, O. J.; Geneste, G.; Yajima, T.; Kobayashi, Y.; Okura, M.; Aidzu, K.; Tassel, C.; Paofai, S.; Swain, D.; Ritter, C.; Kageyama, H., Site Selectivity of Hydride in Early-Transition-Metal Ruddlesden–Popper Oxyhydrides. *Inorg. Chem.* **2018,** *57* (17), 11058-11067.
26. Stephens, P., Phenomenological model of anisotropic peak broadening in powder diffraction. *J. Appl. Crystallogr.* **1999,** *32* (2), 281-289.
27. Blundred, G. D.; Bridges, C. A.; Rosseinsky, M. J., New oxidation states and defect chemistry in the pyrochlore structure. *Angew. Chem. Int. Ed. Engl.* **2004,** *43* (27), 3562-5.
28. Pussacq, T.; Kabbour, H.; Colis, S.; Vezin, H.; Saitzek, S.; Gardoll, O.; Tassel, C.; Kageyama, H.; Laberty Robert, C.; Mentré, O., Reduction of $Ln_2Ti_2O_7$ Layered Perovskites: A Survey of the Anionic Lattice, Electronic Features, and Potentials. *Chem. Mater.* **2017,** *29* (3), 1047-1057.
29. Atuchin, V. V.; Gavrilova, T. A.; Grivel, J. C.; Kesler, V. G., Electronic structure of layered ferroelectric high-ktitanate $La_2Ti_2O_7$. *J. Phys. D: Appl. Phys.* **2008,** *42* (3), 035305.
30. Atuchin, V. V.; Kesler, V. G.; Pervukhina, N. V.; Zhang, Z., Ti 2p and O 1s core levels and chemical bonding in titanium-bearing oxides. *J. Electron. Spectrosc. Relat. Phenom.* **2006,** *152* (1-2), 18-24.

Table of Contents

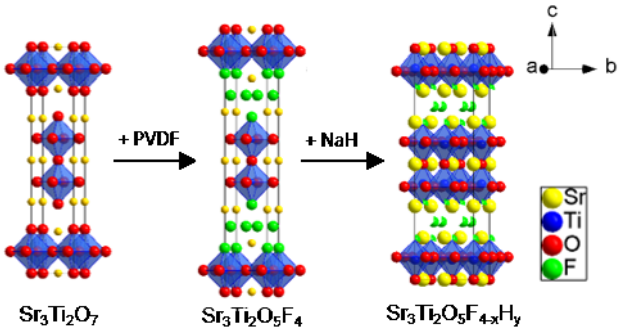

The topochemical fluorination of n = 2 Ruddlesden-Popper type $Sr_3Ti_2O_7$ to $Sr_3Ti_2O_5F_4$ and its subsequent reductive defluorination were investigated. A series of reduction experiments with varying amounts of NaH allowed identifying differently strong reduced phases present in multiphase mixtures using X-ray diffraction. Structural characterization of $Sr_3Ti_2O_5F_4$ and selected reduction products was performed using coupled Rietveld analysis of neutron and X-ray diffraction data. Changes in oxidation states were examined using magnetic measurement and X-ray photoelectron spectroscopy.